# Analysis and mitigation of participation factors weak robustness in direct-drive wind farms connected to VSC-HVDC system

Shao, Bingbing; Wang, Liyuan; Chen, Zhe; Blaabjerg, Frede

*Published in:*
International Journal of Electrical Power & Energy Systems

*DOI (link to publication from Publisher):*
10.1016/j.ijepes.2023.109311



*Publication date:*
2023

*Document Version*
Publisher's PDF, also known as Version of record

Electrical Power and Energy Systems 153 (2023) 109311

Contents lists available at ScienceDirect

International Journal of Electrical Power and Energy Systems

journal homepage: www.elsevier.com/locate/ijepes

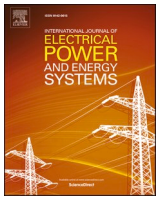

# Analysis and mitigation of participation factors weak robustness in direct-drive wind farms connected to VSC-HVDC system

Bingbing Shao [a,*], Liyuan Wang [b], Zhe Chen [c], Frede Blaabjerg [c]

[a] Anhui Province Key Laboratory of Renewable Energy Utilization and Energy Saving (Hefei University of Technology), Hefei 230009, China
[b] State Grid Changfeng County Electric Power Supply Company, Hefei 231131, China
[c] Department of Energy Technology, Aalborg University, Aalborg DK-9220, Denmark

ARTICLE INFO

*Keywords:*
Close modes
Participation factor
Sub-synchronous oscillation
VSC-HVDC
Weak robustness
Wind farm

ABSTRACT

The participation factors of close sub-synchronous oscillation modes in direct-drive wind farms connected to VSC-HVDC system are greatly affected by parameter perturbations. This affects the damping controller optimal configuration. In light of the issue, participation factors weak robustness is revealed with the matrix perturbation method, and its negative impact on damping controllers is explained. Then, the participation factors weak robustness phenomenon and its hazards are analyzed. Finally, a mitigation method of participation factors weak robustness is proposed. PSCAD/EMTDC simulations are conducted to verify the analysis results.

## 1. Introduction

The VSC-HVDC system has been found to offer both technical and economic advantages for large-scale wind power consumption [1,2]. Moreover, the direct-drive permanent magnetic synchronous generator (PMSG) has several benefits, including ease of maintenance and high efficiency. Consequently, direct-drive wind farms connected to VSC-HVDC system (DDWFV) is now the preferred way for long-distance wind power transmission. However, the sub-synchronous oscillations (SSOs) related to these projects are increasingly becoming a concern [3–5], as the SSOs may lead to instability incidents and poor quality issues.

The SSOs of the DDWFV are typically investigated using the single-machine model [6–10]. However, the SSO characteristics in the multi-machine model differ from those observed in the single-machine model [11], and the oscillations that occur inside wind farms cannot be adequately represented with the single-machine model [12]. It was observed that an *n*-machine DDWFV system has one wind-farm-grid SSO mode that is influenced by both the wind power generation systems and the outer grid, as well as *n*-1 inside-wind-farm SSO modes that are influenced only by the wind power generation systems and not the outer grid [13]. In the case of a homogeneous wind farm, its inside-wind-farm SSO modes are closely spaced [14].

Early research on close modes (CMs) originated in the field of mechanical vibration, including the identification, analysis, and control of CMs [15–17]. In the power systems field, the low-frequency oscillation (LFO) modes dominated by thermal power units occur in the frequency range of 0.1–2.5 Hz. When two LFO modes approach each other, the nearby strong resonance and nearby weak resonance emerge. I. Dobson analyzed this phenomenon and found that under the nearby strong resonance, the moving direction of two low-frequency CMs may vary greatly with parameter changes [18]. However, under the nearby weak resonance, the moving direction of two low-frequency CMs remains unchanged under parameter perturbations [19]. The open-loop modal resonance analysis (OMA) method, proposed by H. Wang, splits a system into two subsystems and examines the SSOs from the perspective of modal information. This approach attributes the oscillation risk to the proximity of the open-loop modes in the two subsystems. Closely spaced open-loop modes may lead to weakly-damped or negatively-damped closed-loop modes, resulting in system instability.

In summary, the concepts of nearby strong resonance [18], nearby weak resonance [19], and open-loop modal resonance [20] aim to describe the changes in the movement trajectory of CMs. A. P. Seyranian and I. Dobson proposed the idea of strong modal resonance, which indicates that if two modes are closely spaced and their eigenvectors are linearly related, the movement trajectory of the two modes will change significantly, and one of the two modes may become negatively damped [16,18]. H. Wang proposed the concept of open-loop modal resonance, which describes the changes of closed-loop modes due to the interaction between two open-loop modes. At the open-loop modal resonance point,

* Corresponding author.
*E-mail address:* shaobingbing1223@163.com (B. Shao).

https://doi.org/10.1016/j.ijepes.2023.109311
Received 6 February 2023; Received in revised form 17 May 2023; Accepted 11 June 2023
Available online 17 June 2023

the corresponding closed-loop modes may become poorly damped [20]. However, the changes in participation factors (PFs) of CMs seem to have been neglected in power system analysis. The changes in mode movement trajectories affect system stability analysis, while the changes in PFs affect the optimal configuration of damping controllers. Since the PFs reflect the participation degrees of state variables to modes, the optimal locations for damping controllers are the wind turbine generators (WTGs) with large PFs. A conference paper presented a phenomenon called PFs weak robustness (PFWR) [21], which refers to the significant changes in power system modes resulting from small parameter perturbations. However, the conditions that trigger the PFWR are not entirely revealed, and there is a lack of PFWR mitigation methods. In the event that the PFWR does occur, the dominant WTGs and the optimal location of damping controllers may change, and the initially installed damping controllers may perform inadequately. It is important to note that the proposed mitigation method in the paper aims to suppress the PFWR rather than mitigate the oscillations of the DDWFV. Three typical methods are used to address oscillations: adding flexible AC transmission system (FACTS) equipment, optimizing parameters, and adding damping controllers [22]. However, these methods cannot mitigate the PFWR as the PFWR results from highly-sensitive PFs rather than weakly-damped oscillation modes. Previous studies have focused on mitigating the nearby strong resonance in thermal power generation systems by avoiding the appearance of CMs. To eliminate the CMs, the parameters of static synchronous series compensator (SSSC), power system stabilizer (PSS), and static synchronous compensator (STATCOM) were adjusted [23–25]. Similarly, improvements in HVDC modulation control have been made to eliminate CMs in synchronous generators connected to HVDC systems [26]. However, the influencing factors of nearby strong resonance in thermal power generation systems and the PFWR in wind farm grid-connected systems are distinct. Moreover, the adjustment of a single control loop in previous studies [23–26] may not increase the distances of a large number of modes. In light of these gaps, this paper aims to further elucidate the triggering conditions and negative impacts of PFWR, and proposes a PFWR mitigation method of the DDWFV.

The remaining sections of this paper are structured as follows. Section 2 reveals the mechanism of PFWR. Section 3 presents the PFWR phenomenon and its adverse effects on damping controllers with a three-machine DDWFV system. In Section 4, the mitigation method of PFWR is proposed. Section 5 further discusses the PFWR mechanism, phenomenon, and mitigation method. Finally, Section 6 provides the concluding remarks.

## 2. Participation factors weak robustness mechanism

### 2.1. Triggering conditions of participation factors weak robustness

With the matrix perturbation method, the state matrix $\boldsymbol{A}(\varepsilon)$, eigenvalue $\lambda_i(\varepsilon)$ and right eigenvector $\boldsymbol{U}_i(\varepsilon)$ are expressed as [27]:

$$\begin{cases} \mathbf{A}(\varepsilon) = \mathbf{A} + \varepsilon\mathbf{A}_0 \\ \lambda_i(\varepsilon) = \lambda_i + k_1\varepsilon + k_2\varepsilon^2 + \ldots \\ \mathbf{U}_i(\varepsilon) = \mathbf{U}_i + \varepsilon\sum_{j=1}^{n} s_{j1}\mathbf{U}_j + \varepsilon^2\sum_{j=1}^{n} s_{j2}\mathbf{U}_j + \ldots \end{cases} \tag{1}$$

where $\boldsymbol{A}$, $\lambda_i$, and $\boldsymbol{U}_i$ are the initial state matrix, eigenvalue, and right eigenvector; $\varepsilon$ is a small parameter perturbation quantity; $\varepsilon\boldsymbol{A}_0$ is the perturbation quantity of $\boldsymbol{A}$; $k_i$ and $s_{ji}$ ($i = 1, 2, \ldots, n$) are the perturbation factors of eigenvalue $\lambda_i$ and right eigenvector $\boldsymbol{U}_j$, respectively; $\boldsymbol{U}_j$ is the right eigenvector corresponding to eigenvalue $\lambda_j$; $n$ is the order of state matrix.

Referring to [21], the first-order perturbation factor of right eigenvector is expressed as:

$$s_{j1} = \frac{\mathbf{V}_j^{\mathrm{T}}\mathbf{A}_0\mathbf{U}_i}{(\lambda_i - \lambda_j)} \tag{2}$$

Meanwhile, it can be known from (1) that the derivative of $\boldsymbol{U}_i(\varepsilon)$ with respect to $\varepsilon$ is:

$$\frac{\mathrm{d}\mathbf{U}_i(\varepsilon)}{\mathrm{d}\varepsilon} = \sum_{j=1}^{n} s_{j1}\mathbf{U}_j + 2\varepsilon\sum_{j=1}^{n} s_{j2}\mathbf{U}_j + \ldots \approx \sum_{j=1}^{n} s_{j1}\mathbf{U}_j \tag{3}$$

It can be known from (1) that the main perturbation component of right eigenvector is $\varepsilon\sum_{j=1}^{n} s_{j1}\mathbf{U}_j$, as the other perturbation components are the high-order infinitesimals of this component. $\varepsilon$ is the perturbation quantity, and $s_{j1}$ is affected by the distance between modes ($\lambda_i$ - $\lambda_j$). Therefore, in addition to the parameter perturbation quantity, the distance between modes also affects the right eigenvector. If multiple eigenvalues are closely spaced, $s_{j1}$ will approach infinity and $\mathrm{d}\boldsymbol{U}_i(\varepsilon)/\mathrm{d}\varepsilon$ will be large. A large $\mathrm{d}\boldsymbol{U}_i(\varepsilon)/\mathrm{d}\varepsilon$ implies that the right eigenvector $\boldsymbol{U}_i(\varepsilon)$ is sensitive to parameter perturbations. Then, the left eigenvector ($\boldsymbol{V}_i = \boldsymbol{U}^{-\mathrm{T}}{}_i$) and PF ($\boldsymbol{P}_i = \boldsymbol{U}_i\boldsymbol{V}_i$) of close eigenvalues are also sensitive to parameter perturbations [28]. Therefore, the PFWR results from closely spaced modes. A close distance between modes may lead to the PFWR. Meanwhile, $\varepsilon \neq 0$ is the prerequisite of the matrix perturbation method and the equation (3) [27], so the perturbations should be interrelated to CMs. Small distances between modes and related perturbations to CMs are the triggering conditions for the PFWR.

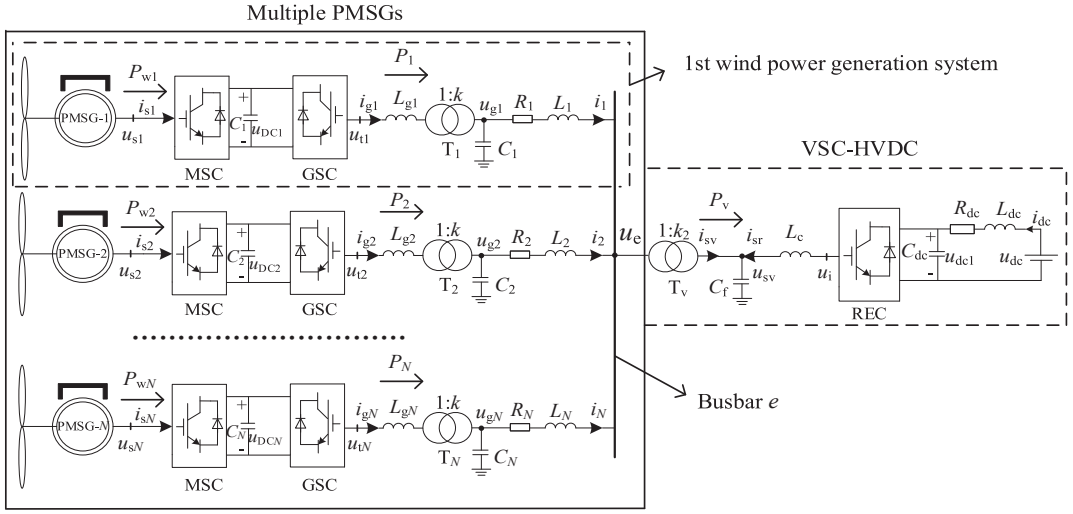


**Fig. 1.** System diagram of direct-drive wind farms connected to VSC-HVDC system (MSC - machine-side converter, GSC - grid-side converter, REC - rectifier).

**Table 1**
Parameters of the three-machine system.

| PMSGs | DC capacitor ($C$), outer loop DC voltage control ($k_{p4}$、$k_{i4}$), filter inductance ($L_g$) |
|---|---|
| PMSG-1 ($v_1 = 11$ m/s) | Initial values in Tables A1 and A2 in Appendix A |
| PMSG-2 ($v_2 = 12$ m/s) | Setting values increased by 5% |
| PMSG-3 ($v_3 = 13$ m/s) | Setting values decreased by 5% |

**Table 2**
SSO modes of the three-machine system.

| SSO modes | Eigenvalues | Oscillation frequency (Hz) | Damping ratio |
|---|---|---|---|
| $\lambda_{1,2}$ | $10.252 \pm j104.14$ | 16.5744 | −0.0980 |
| $\lambda_{3,4}$ | $8.2407 \pm j105.05$ | 16.7192 | −0.0782 |
| $\lambda_{5,6}$ | $8.9056 \pm j104.66$ | 16.6572 | −0.0848 |

With the matrix perturbation method, A. P. Seyranian obtained the derivative of eigenvalue with respect to $\varepsilon$, which distinguishes strong/weak modal interactions [16,29]. However, the happening of PFWR depends on the derivative of PFs with respect to $\varepsilon$, and the PFWR implies highly-sensitive PFs to parameter perturbations, which is different from strong/weak modal interactions. The theoretical proof in [16,29] aims to explain the movement trajectory of CMs, but it cannot reflect the PF changes and reveal the PFWR mechanism.

### 2.2. Negative impact of participation factors weak robustness

$\boldsymbol{P}_{fi}$ ($f = 1, 2, \ldots, n$; $i = 1, 2, \ldots, n$) is defined as the PF of the $i$-th state variable to the $f$-th oscillation mode. The normalized PFs from state variables to oscillation modes satisfy the following relationship [28]:

$$\begin{cases} \mathbf{P}_{11} + \mathbf{P}_{12} + \ldots + \mathbf{P}_{1n} = 1 \\ \mathbf{P}_{21} + \mathbf{P}_{22} + \ldots + \mathbf{P}_{2n} = 1 \\ \quad\quad\quad\quad \ldots\ldots \\ \mathbf{P}_{n1} + \mathbf{P}_{n2} + \ldots + \mathbf{P}_{nn} = 1 \end{cases} \tag{4}$$

It can be known from (4) that the sum of PFs across all state variables involved in a single oscillation mode remains constant ($\sum_{i=1}^{n} \mathbf{P}_{fi} = 1$). As the PFWR may lead to a significant increase in the PFs of certain state variables involved in an oscillation mode, the PFs of other state variables decrease significantly. Consequently, the dominant state variables and WTGs participating in the oscillation mode may shift after parameter perturbations. This shift affects the optimal placement of damping controllers, resulting in poor controller performances, as discussed in the following section.

## 3. Participation factors weak robustness phenomenon and hazards

### 3.1. Participation factors weak robustness phenomenon

In this Section, the PFWR phenomenon is presented with the three-machine DDWFV system, as shown in Fig. 1. The control structures of machine-side converter (MSC), grid-side converter (GSC), rectifier (REC) and phase-locked loop (PLL) adopt the structures in [9]. It can be known from [9] that the inside-wind-farm/wind-farm-grid SSOs of DDWFV are affected by the outer loop DC voltage control of PMSGs, DC capacitor $C$, and filter inductance $L_g$. Considering the parameter differences of PMSGs and the influencing factors of SSOs, certain parameters in the three-machine system are set different, as listed in Table 1. Meanwhile, the SSO modes of the three-machine system are calculated, as listed in Table 2. Table 2 shows that there are three SSO modes in the three-machine system, and the modes are negatively-damped. The

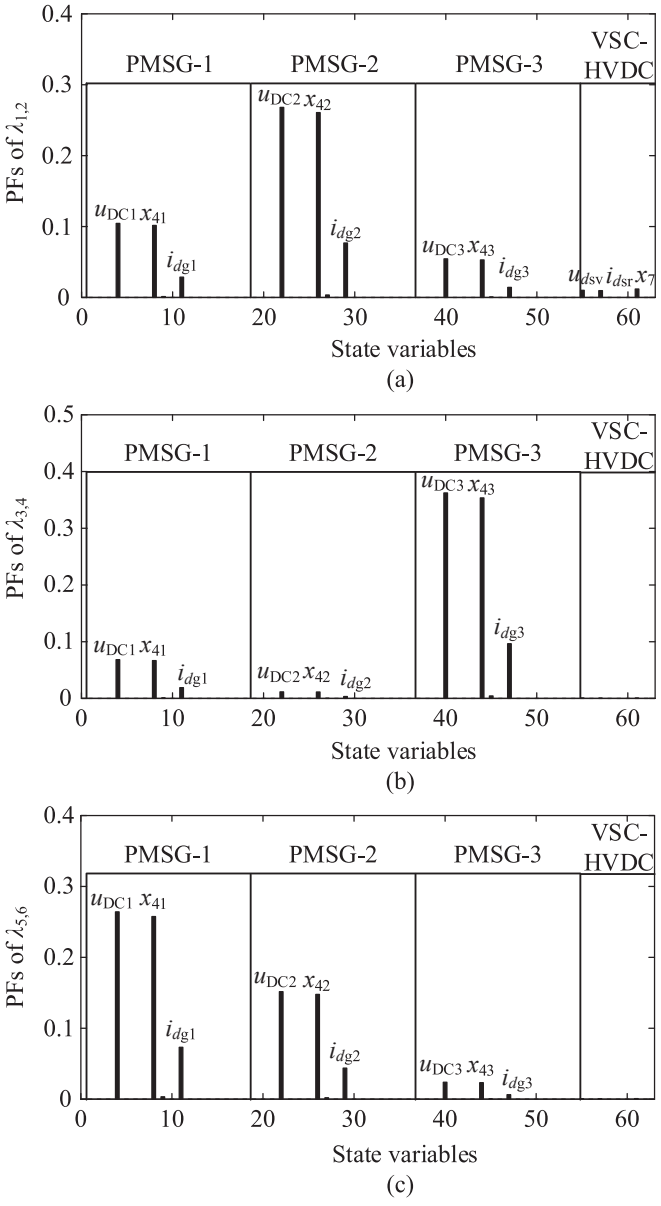


**Fig. 2.** Normalized participation factors (PFs) of the SSO modes in the three-machine system without parameter perturbations: (a) $\lambda_{1,2}$, (b) $\lambda_{3,4}$, and (c) $\lambda_{5,6}$.

**Table 3**
PFs of different PMSGs to the SSO modes when the wind speed is increased by 5% in the three-machine system.

| SSO modes | PMSG-1 | | PMSG-2 | | PMSG-3 | |
|---|---|---|---|---|---|---|
| | Before | After | Before | After | Before | After |
| $\lambda_{3,4}$ | 0.1551 | 0.1457 | 0.0265 | **0.4531** | **0.8168** | **0.4012** |
| $\lambda_{5,6}$ | **0.5985** | 0.2014 | 0.3454 | **0.6071** | 0.0538 | 0.1915 |

normalized PFs of the SSO modes are shown in Fig. 2, where $x_4$ is expressed as:

$$px_4 = u_{DC} - u_{DCref} \tag{5}$$

where $p = d/dt$; $u_{DC}$ is the measure value of dc voltage in back-to-back converter, and $u_{DCref}$ is the reference value.

Fig. 2 indicates that the state variables related to the SSO mode $\lambda_{1,2}$ are $u_{DC}$, $x_4$, $i_{dg}$ in three PMSGs and $u_{dsv}$, $i_{dsr}$, $x_7$ in the VSC-HVDC system. The state variables related to the SSO modes $\lambda_{3,4}$ and $\lambda_{5,6}$ are $u_{DC}$, $x_4$, $i_{dg}$

**Table 4**
PFs of different PMSGs to the SSO modes when the outer loop parameters of DC voltage control are increased by 5% in the three-machine system.

| SSO modes | PMSG-1 | | PMSG-2 | | PMSG-3 | |
|---|---|---|---|---|---|---|
| | Before | After | Before | After | Before | After |
| $\lambda_{3,4}$ | 0.1551 | 0.0546 | 0.0265 | **0.8076** | **0.8168** | 0.1150 |
| $\lambda_{5,6}$ | **0.5985** | 0.0220 | 0.3454 | 0.1060 | 0.0538 | **0.8670** |

**Table 5**
PFs of different PMSGs to the SSO modes when the DC capacitor is increased by 5% in the three-machine system.

| SSO modes | PMSG-1 | | PMSG-2 | | PMSG-3 | |
|---|---|---|---|---|---|---|
| | Before | After | Before | After | Before | After |
| $\lambda_{3,4}$ | 0.1551 | 0.0145 | 0.0265 | 0.0931 | **0.8168** | **0.8880** |
| $\lambda_{5,6}$ | **0.5985** | 0.0883 | 0.3454 | **0.7880** | 0.0538 | 0.1029 |

Before – before parameter perturbations; After – after parameter perturbations.

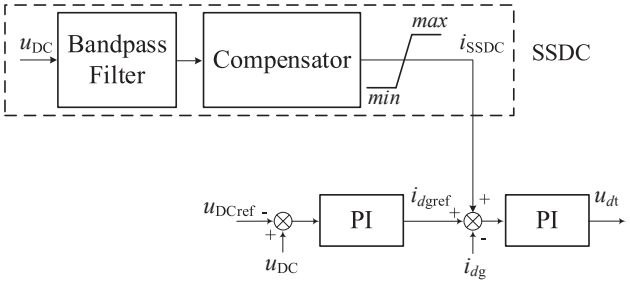


**Fig. 3.** Structure of the sub-synchronous damping controller (SSDC).

in the PMSGs. Therefore, $\lambda_{1,2}$ is a wind-farm-grid SSO mode, and $\lambda_{3,4}$, $\lambda_{5,6}$ are inside-wind-farm SSO modes. To present the PFWR phenomenon in the three-machine system, certain parameters of PMSG-1 are separately increased by 5%. Tables 3–5 list the PFs of different PMSGs to the SSO modes before and after parameter perturbations. The PFs from a PMSG are the sum of the PFs from all the state variables in the PMSG. As the parameter perturbations have little influence on the PFs of wind-farm-grid SSO mode $\lambda_{1,2}$, its PFs are not listed in Tables 3–5 [21]. It can be seen from Tables 3–5 that the PFs of $\lambda_{3,4}$ and $\lambda_{5,6}$ are greatly affected by parameter perturbations. The dominant PMSGs participating in $\lambda_{3,4}$ and $\lambda_{5,6}$ change from PMSG-1 and 3 to PMSG-2 and 3 after the perturbations of wind speed, DC voltage outer loop control parameters and DC capacitor. Therefore, the parameter perturbations greatly affect the PFs and lead to the changes in dominant PMSGs.

It can be known from the above analysis that the PFs of inside-wind-farm SSO modes change greatly after parameter perturbations. As there are two close inside-wind-farm SSO modes in the three-machine system, $\mathrm{d}\boldsymbol{U}_i(\varepsilon)/\mathrm{d}\varepsilon$ in (3) corresponding to the two modes is large. Meanwhile, as the wind-farm-grid SSO mode is far from the inside-wind-farm SSO modes, its $\mathrm{d}\boldsymbol{U}_i(\varepsilon)/\mathrm{d}\varepsilon$ in (3) is small. The PFWR phenomenon presented in this section is in consistent with the mechanism analysis in Section 2.

### 3.2. Participation factors weak robustness hazards

In order to illustrate the detrimental effects of PFWR on damping controllers, the sub-synchronous damping controller (SSDC) in [30] is adopted. The structure of SSDC is shown in Fig. 3. Since the SSOs in the DDWFV are greatly affected by the DC voltage control of PMSGs, the output signal of SSDC ($i_{SSDC}$) is added to the DC voltage inner loop control of the GSC. The SSDC consists of a filter, a compensator, and a limiter. The filter loop extracts the oscillation component of input variables with a fourth-order Butterworth band-pass filter. The center

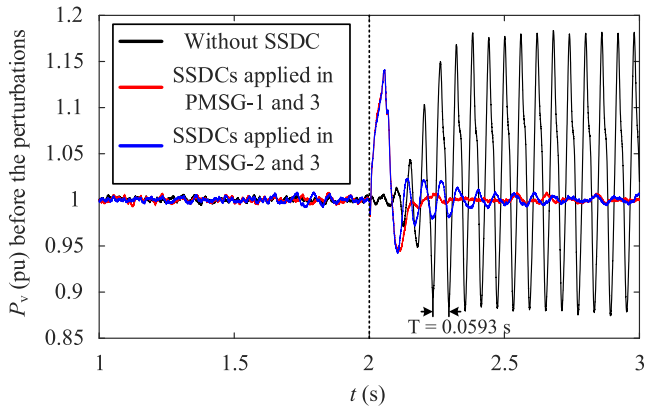


**Fig. 4.** Output active power ($P_v$) before the parameter perturbations with SSDCs applied in different PMSGs.

frequency of the filter is set to the SSO frequency, and the bandwidth is the frequency range of SSO. The compensator of the SSDC is expressed in (6) and includes a phase shifter component and a constant gain. The phase shifter component adopts a series correction form, including a lagging loop and a leading loop. The lagging loop effectively improves steady-state performances, while the leading loop has a large bandwidth and fast response. As the SSDC cannot affect the system stable operation, a limiter is added to the SSDC [31]. The parameters of the SSDC are designed based on the role of different components and are listed in Table A3 in Appendix.

$$T(s) = \underbrace{G}_{gain} \underbrace{\left(\frac{sT_{11}+1}{sT_{12}+1}\right)^{m}\left(\frac{sT_{21}+1}{sT_{22}+1}\right)^{n}}_{Phase\ \ shifters}, T_{11} > T_{12} \text{ and } T_{21} < T_{22} \tag{6}$$

Tables 3–5 show that before the perturbations of wind speed, DC voltage outer loop control parameters and DC capacitor, the dominant PMSGs are PMSG-1, 3. After the parameter perturbations, the dominant PMSGs change to PMSG-2, 3. Therefore, the optimal locations of SSDCs before the parameter perturbations are PMSG-1, 3, while the optimal locations of SSDCs after the parameter perturbations are PMSG-2, 3.

To demonstrate the changes in the optimal locations of SSDCs, the SSDCs are applied in PMSG-1 and 3 or PMSG-2 and 3 before and after the parameter perturbations. The simulation model of the DDWFV is built in PSCAD/EMTDC software, with a sampling size of 20 μs, and the solver is Fortran Compiler. When a three-phase short-circuit ground fault happens in the busbar $e$ at $t = 2$ s and is cleared after 50 ms, the output active power ($P_v$) before and after the parameter perturbations in the three-machine system is shown in Figs. 4 and 5. It can be seen from Fig. 4 that the SSDCs can effectively improve the SSO damping compared with the condition without SSDCs. Before the parameter perturbations, Fig. 4 shows that the SSDCs applied in PMSG-1 and 3 perform better than the SSDCs applied in PMSG-2 and 3. However, after the parameter perturbations, Fig. 5 shows that the SSDCs applied in PMSG-2 and 3 perform better than the SSDCs applied in PMSG-1 and 3. It can be seen from Fig. 5 (a) and (c) that if the location of SSDCs remains unchanged after the perturbations, the SSDCs will fail to mitigate the SSOs, and the SSOs will become divergent. Therefore, due to the PFWR, the initial location of SSDCs may not be optimal after the parameter perturbations. Under parameter perturbations, the PFWR makes the performances of SSDCs worse and even fail to mitigate the SSOs.

### 3.3. Participation factors sensitivity analysis

With the PFs sensitivities defined in [21], The PFs sensitivities of PMSGs to dominant oscillation modes are calculated, as shown in Fig. 6.

It can be seen from Fig. 6 that the PFs sensitivities to $\lambda_{3,4}$ and $\lambda_{5,6}$ are much larger than that to $\lambda_{1,2}$. The PFs sensitivities from three PMSGs to

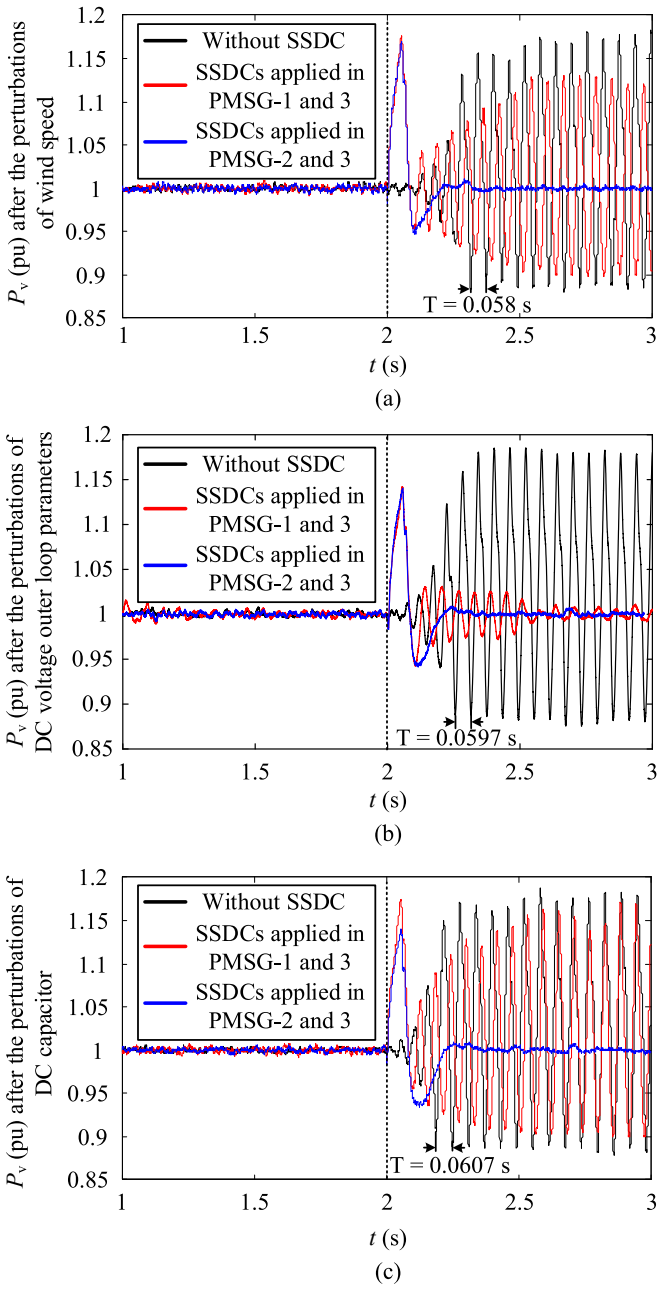


**Fig. 5.** Output active power ($P_v$) after the parameter perturbations with SSDCs applied in different PMSGs: (a) after the perturbations of wind speed, (b) after the perturbations of DC voltage outer loop control parameters and (c) after the perturbations of DC capacitor.

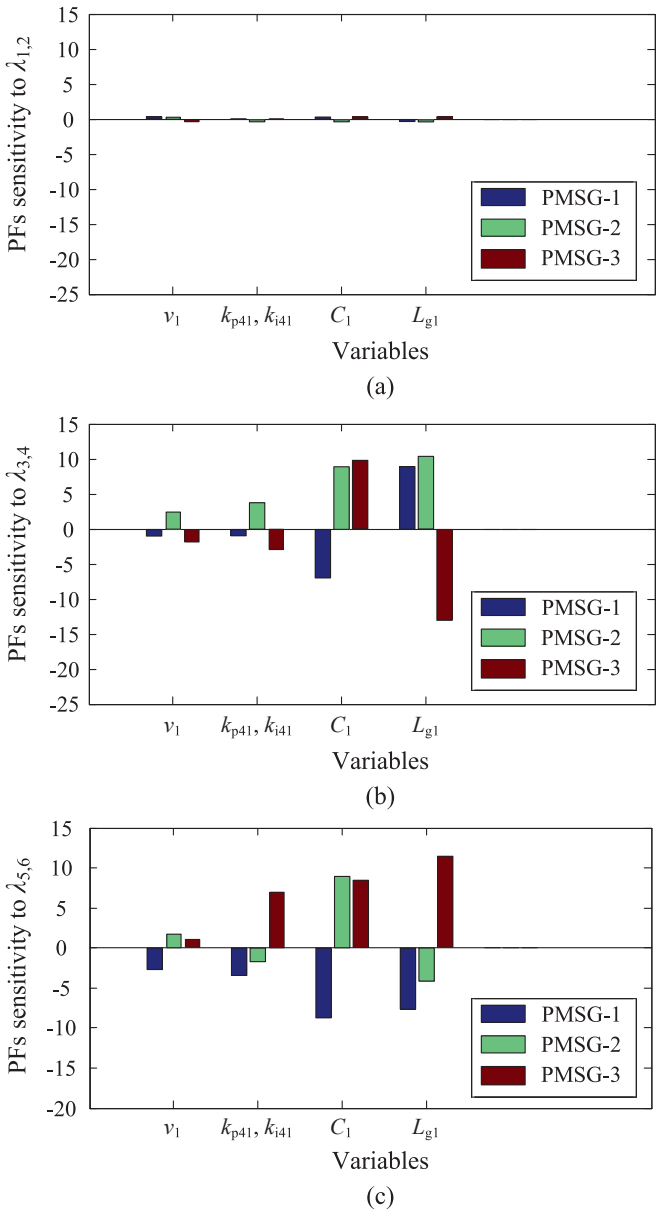


**Fig. 6.** PFs sensitivities of PMSGs to dominant oscillation modes $\lambda_{1,2}$ - $\lambda_{5,6}$: (a) $\lambda_{1,2}$, (b) $\lambda_{3,4}$ and (c) $\lambda_{5,6}$.

$\lambda_{1,2}$ are nearly 0, as $\lambda_{1,2}$ is far from other modes and (2), (3) are small. The quantities and directions of PFs sensitivities from three PMSGs to close SSO modes $\lambda_{3,4}$ and $\lambda_{5,6}$ are different. For example, under the wind speed perturbation, the PFs sensitivity from PMSG-1 and 3 to $\lambda_{3,4}$ is negative, while the PFs sensitivity from PMSG-2 to $\lambda_{3,4}$ is positive. This indicates that under wind speed perturbations, part PFs to $\lambda_{3,4}$ will transfer from PMSG-1 and 3 to PMSG-2.

## 4. Participation factors weak robustness mitigation

*Dynamically Adjust Damping Controllers based on the Analytical Solution of PFs under Parameter Perturbations:* Based on multiple sampling points, the analytical expression of the PFs under parameter perturbations can be obtained by curve fitting (polynomial approximation, linear fitting, etc.). Then, the damping controller can be dynamically adjusted according to the analytical expression of PFs. This method does not need much investment, and the calculation workload is dominated by the one-time curve fitting process. Therefore, the method does not require repeated small-signal modeling, and the calculation amount and delay are small. However, the analytical expression of PFs based on the curve fitting is hard to cover full operating conditions, and thus its solution accuracy is under doubt. The optimal location of damping controllers depends on the PFs from different PMSGs, so it is vital to obtain the analytical expression of the PFs from different PMSGs.

(1) *Polynomial Fitting:* Defining the PFs of the $j$-th PMSG to the $i$-th mode as $\boldsymbol{P}_{j|i}$. To obtain the analytical expression of $\boldsymbol{P}_{j|i}$, a polynomial can be used to fit the expression of PFs [32], as shown as:

$$\mathbf{P}_{j|i}(\mathbf{a}) \approx \mathbf{Q}_{j|i}(\mathbf{a}) = \mathbf{P}_{j|i}(\mathbf{a}_0) + \mathbf{P}^{(1)}_{j|i}(\mathbf{a}_0)(\mathbf{a}-\mathbf{a}_0)^1 + \ldots + \frac{\mathbf{P}^{(m)}_{j|i}(\mathbf{a}_0)(\mathbf{a}-\mathbf{a}_0)^m}{m!} \quad (7)$$

where $\boldsymbol{a}_0$ is the initial system parameter; $\boldsymbol{P}^{(m)}_{j|i}$ denotes the $m$-order

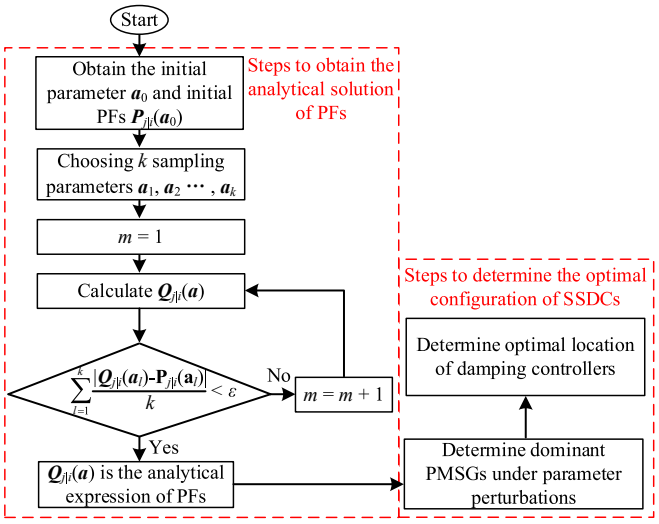


**Fig. 7.** Flow chart of the damping controller optimal configuration based on the analytical solution of PFs.

**Table 6**
Analytical expression of PFs from different PMSGs to close SSO modes under the DC capacitor perturbations in PMSG-1.

| | Analytical expression and corresponding calculation error in the bracket |
|---|---|
| $Q_{1\|1}(C)$ | $(5.969 \times 10^{-7})C^4$-$(8.406 \times 10^{-5})C^3 + 0.004297C^2$-$0.09426C + 0.7465$ (≈0) |
| $Q_{2\|1}(C)$ | $(8.896 \times 10^{-7})C^4$-$0.0001084C^3 + 0.004551C^2$-$0.06623C + 0.3327$ (≈0) |
| $Q_{3\|1}(C)$ | $(8.108 \times 10^{-6})C^3$-$0.000799C^2 + 0.02635C + 0.625$ (0.005797) |
| $Q_{1\|2}(C)$ | $(2.298 \times 10^{-6})C^4$-$0.0003236C^3 + 0.01655C^2$-$0.363C + 2.875$ (≈0) |
| $Q_{2\|2}(C)$ | $(-2.522 \times 10^{-6})C^4 + 0.0003476C^3$-$0.0173C^2 + 0.3689C$-$1.936$ (≈0) |
| $Q_{3\|2}(C)$ | $(-6.204 \times 10^{-7})C^4$+$(7.886 \times 10^{-5})C^3$-$0.003433C^2 + 0.06715C$-$0.3478$ (≈0) |

derivative of $P_{j|i}$ to $a$, and $m$ is less than or equal to the order of DDWFV. $Q_{j|i}(a)$ is the analytical expression of $P_{j|i}(a)$.

With the increase of $m$, the error between $P_{j|i}(a)$ and $Q_{j|i}(a)$ may be smaller, but the amount of calculation becomes larger. Therefore, $m$ needs to be determined considering both the calculation error and calculation quantity. The steps to obtain the analytical solution of PFs are shown in Fig. 7, where $\varepsilon$ is the maximum allowable error.

In Fig. 7, the first step is to calculate the initial PFs $P_{j|i}(a_0)$ with the modal analysis. With typical $k$ sampling parameters $a_1$-$a_k$ and $m = 1$, the average error of the analytical expression is calculated with $\sum_{l=1}^{k} \frac{|Q_{j|i}(a_l)-P_{j|i}(a_l)|}{k}$. If the error is less than the maximum allowable error $\varepsilon$, $Q_{j|i}(a)$ with $m = 1$ is the analytical solution of PFs. Otherwise, $m$ increases until the error is less than $\varepsilon$, and then $Q_{j|i}(a)$ with such $m$ can be obtained.

(2) *Analytical Calculation:* With the three-machine system in Section 3, the analytical PFs of PMSGs to close SSO modes can be calculated according to Fig. 7. The perturbations of the DC capacitor in PMSG-1 are taken as an example. $Q_{j|1}$ is defined as the analytical expression of the PFs from $j$-th PMSG to the SSO mode $\lambda_{3,4}$, and $Q_{j|2}$ is defined as the analytical expression of the PFs from $j$-th PMSG to the SSO mode $\lambda_{5,6}$. In Fig. 7, the maximum allowable error ($\varepsilon$) is set to 0.01, and the sampling parameters are selected as $C = 10$ mF, 20 mF, 30 mF, 40 mF, and 50 mF. After the polynomial fitting of PFs according to the steps in Fig. 7, the analytical expression of PFs under DC capacitor perturbations is shown in Table 6.

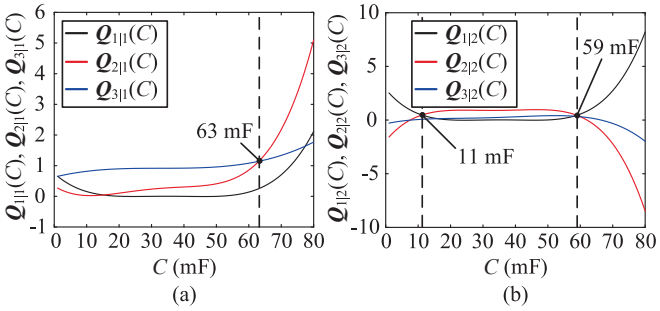


**Fig. 8.** Analytical expressions of the PFs from different PMSGs to the close SSO modes $\lambda_{3,4}$ or $\lambda_{5,6}$: (a) PFs to $\lambda_{3,4}$ and (b) PFs to $\lambda_{5,6}$.

**Table 7**
Dominant PMSGs participating in close SSO modes according to the analytical expressions of PFs.

| $C$ | 0 – 11 mF | 11 – 59 mF | 59 – 63 mF | > 63 mF |
|---|---|---|---|---|
| Dominant PMSGs to $\lambda_{3,4}$ | PMSG-3 | PMSG-3 | PMSG-3 | PMSG-2 |
| Dominant PMSGs to $\lambda_{5,6}$ | PMSG-1 | PMSG-2 | PMSG-1 | PMSG-1 |
| Optimal SSDCs' locations | PMSG-1, 3 | PMSG-2,3 | PMSG-1,3 | PMSG-1,2 |

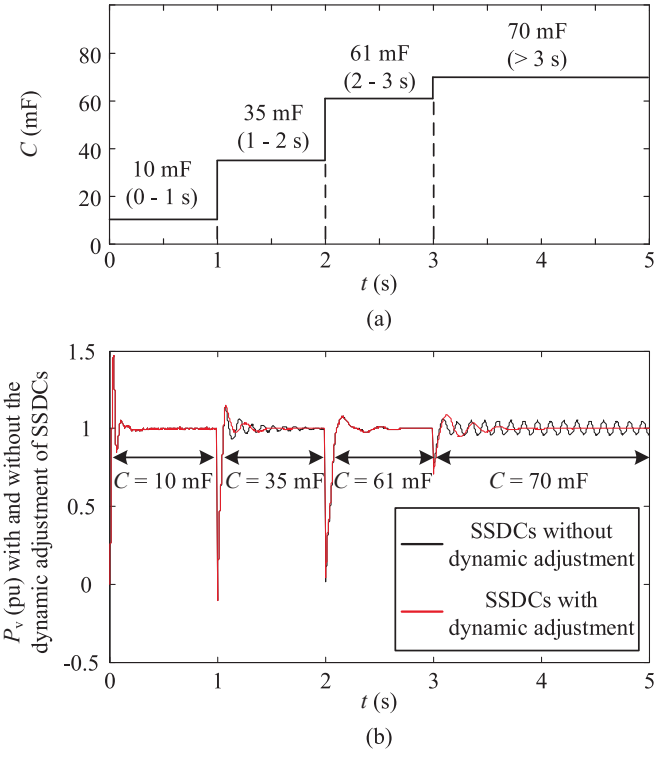


**Fig. 9.** The performances of SSDCs under DC capacitor ($C$) perturbations with and without dynamic adjustment: (a) the perturbations of $C$ over time and (b) output active power ($P_v$) with and without dynamic adjustment of SSDCs.

(3) *Damping Controller Optimal Configuration:* With the analytical expression of PFs, the steps to obtain the optimal configuration of SSDCs are shown in Fig. 7. The dominant PMSGs with large PFs can be obtained by plotting the analytical expressions of PFs from different PMSGs together, as shown in Fig. 8. It can be known from Fig. 8 that certain intersections of different analytical

expressions determine the dominant PMSGs with the largest PFs, which is listed in Table 7. Table 7 shows that the optimal locations of SSDCs are different with different DC capacitors, which implies that the SSDCs need to be dynamically adjusted under DC capacitor perturbations.

To present the performance of SSDCs with dynamic adjustment based on the analytical solution of PFs, the perturbations of $C$ are set as shown in Fig. 9(a). The performances of SSDCs are compared with and without dynamic adjustment, as shown in Fig. 9(b). The SSDCs without dynamic adjustment imply that the locations of SSDCs keep unchanged when DC capacitor changes, and the SSDCs with dynamic adjustment imply that the locations of SSDCs are dynamically adjusted according to Table 7 when DC capacitor changes. It can be seen from Table 7 that the optimal locations of SSDCs when $C = 35$ mF and 70 mF are different from the initial optimal locations when $C = 10$ mF. Therefore, it can be known from Fig. 9 that when $C = 35$ mF and 70 mF, the damping of output active power without the dynamic adjustment of SSDCs is smaller than that with the dynamic adjustment of SSDCs. When $C = 70$ mF, the SSDCs without the dynamic adjustment fail to mitigate the SSOs. Therefore, dynamically adjusting SSDCs based on the analytical PFs helps to improve the system damping and the robustness of SSDCs.

## 5. Discussion

The PFWR mechanism, phenomenon, and mitigation method are further discussed as follows:

(1) *PFWR Mechanism:* In Section 2, the PFWR mechanism analysis revealed that the PFs of closely spaced oscillation modes are highly sensitive to parameter perturbations. However, the analysis was based on matrix perturbation theory and lacked a clear physical interpretation. Further research is necessary to understand why closely spaced oscillation modes lead to PFWR from a physical perspective.
(2) *PFWR Phenomenon:* CMs can also appear in photovoltaic grid-connected systems or different regional power grids. Thus, the PFWR phenomenon may also occur in other renewable energy systems and regional interconnected power grids. Further research is required to investigate this possibility.
(3) *PFWR Mitigation:* The effect of dynamically adjusting the SSDCs relies on the PFs calculation speed and accuracy. The PFs calculation speed can be improved with a high-performance computer or by reducing the order of small-signal model. Meanwhile, the accuracy of PFs analytical expression can be improved by setting maximum allowable error ($\varepsilon$) smaller or being fitted with more sampling points.
(4) *Differences Among PFWR, Nearby Strong Resonance, and Nearby Weak Resonance:* Although the PFWR, nearby strong resonance, and nearby weak resonance all result from close modes, their characteristics differ. Nearby strong resonance is a specific case of open-loop modal resonance when the parameter variation is zero [33]. The PFWR describes the change in PFs of CMs under parameter perturbations, while the nearby strong resonance and nearby weak resonance describe changes in the moving direction of CMs under parameter perturbations. Therefore, nearby strong resonance/nearby weak resonance can guide system stability analysis, while the PFWR can guide the design of damping controllers.

## 6. Conclusion

In this paper, we propose triggering conditions and a mitigation method for participation factor weak robustness in direct-drive wind farms connected to VSC-HVDC system. Main concluding remarks are summarized as follows:

**Table A1**
Parameters of PMSG power generation system.

| Components | Variables | Value |
|---|---|---|
| WTG | Rated power (MW) | $40 \times 5$ |
| | Rotor flux (Wb) | 0.0417 |
| | Stator resistance (Ω) | 0.0950 |
| | Stator inductance (H) | 0.0121 |
| | DC capacitor $C$ (mF) | 12 |
| MSC | Unity power factor control coefficient (proportional $k_{p1}$, integral $k_{i1}$) | 1, 5 |
| | Speed control outer loop coefficient (proportional $k_{p2}$, integral $k_{i2}$) | 0.4, 2.5 |
| | Speed control inner loop coefficient (proportional $k_{p3}$, integral $k_{i3}$) | 1, 5 |
| GSC | DC voltage control outer loop coefficient (proportional $k_{p4}$, integral $k_{i4}$) | 0.2, 400 |
| | DC voltage control inner loop coefficient (proportional $k_{p5}$, integral $k_{i5}$) | 0.6, 2.5 |
| | $q$-axis current control coefficient (proportional $k_{p6}$, integral $k_{i6}$) | 0.6, 2.5 |
| PLL | Proportional $k_{p\_pll}$, integral $k_{i\_pll}$ | 50, 100 |
| Collector transmission lines | Filter inductor $L_g$ (H) | 0.002 |
| | Line resistance $R$ (Ω) | 0.05 |
| | Line inductance $L$ (H) | 0.001 |
| | Line capacitance $C$ (μF) | 2 |

(1) When there are close sub-synchronous oscillation modes in direct-drive wind farms connected to VSC-HVDC system and perturbations are related to these modes, the participation factors of these modes become sensitive to parameter perturbations, leading to participation factor weak robustness.
(2) Participation factor weak robustness can cause changes of the dominant PMSGs participating in close sub-synchronous oscillation modes under parameter perturbations, which affects the optimal locations and performance of damping controllers.
(3) To eliminate or reduce the hazards of participation factor weak robustness, dynamically adjusting the damping controller locations according to the analytical solution of participation factors can help improve the robustness of damping controllers.

Participation factors weak robustness mechanism and mitigation methods can be also applied in photovoltaic grid-connected systems and regional interconnected power grids with close modes, since the participation factors weak robustness theory is a general account of typical system behaviors with close modes. Meanwhile, the physical mechanism of PFWR remains to be investigated. The relevant conclusions help to deepen the understanding of the system with close modes, and the robustness of damping controllers under parameter perturbations can be improved through the proposed method. Certain viewpoints need to be changed: instead of only examining the participation factors of a dominant mode, the hazards of participation factors weak robustness when there are close modes should be considered while trying to stabilize the system.

## CRediT authorship contribution statement

**Bingbing Shao:** Conceptualization, Methodology, Software. **Liyuan Wang:** Writing – original draft. **Zhe Chen:** Writing – review & editing, Supervision. **Frede Blaabjerg:** Writing – review & editing, Supervision.

## Declaration of Competing Interest

The authors declare that they have no known competing financial

**Table A2**
Parameters of VSC-HVDC.

| Components | Variables | Value |
|---|---|---|
| AC-side | Filter capacitor $C_f$ (μF) | 5 |
| | Phase inductance $L_c$ (H) | 0.015 |
| REC | $d$-axis voltage control outer loop coefficient (proportional $k_{p9}$) | 0.0029 |
| | $q$-axis voltage control outer loop coefficient (proportional $k_{p10}$) | 0.0029 |
| | $d$-axis voltage control inner loop coefficient (proportional $k_{p7}$, integral $k_{i7}$) | 2.5, 10,000 |
| | $q$-axis voltage control inner loop coefficient (proportional $k_{p8}$, integral $k_{i8}$) | 2.5, 10,000 |
| DC-side | Resistance $R_{dc}$ (Ω) | 0.006 |
| | Inductance $L_{dc}$ (H) | 0.0005 |
| | Capacitance $C_{dc}$ (μF) | 150 |
| | Equivalent DC voltage source $u_{dc}$ (kV) | 160 |

**Table A3**
Parameters of SSDC.

| Modules | Variables | Value |
|---|---|---|
| Bandpass filter | Center frequency (Hz) | 16 |
| | Bandwidth (Hz) | 4 |
| Compensator | $G$ | 2 |
| | $T_{11}$ | 3.4 |
| | $T_{12}$ | 1.4 |
| | $T_{21}$ | 0.6 |
| | $T_{22}$ | 1.1 |
| | $m$ | 1 |
| | $n$ | 1 |
| Limiter | Amplitude (p.u.) | 0.1 |

interests or personal relationships that could have appeared to influence the work reported in this paper.

## Data availability

No data was used for the research described in the article.

## Appendix A

See Table A1, Table A2, Table A3.

## References


[1] Korompili A, Wu Q, Zhao H. Review of VSC HVDC connection for offshore wind power integration. Renew Sust Energ Rev 2016;59:1405–14.
[2] Shao B, Xiao Q, Xiong L, Wang L, Yang Y, Chen Z, et al. "Power coupling analysis and improved decoupling control for the VSC connected to a weak AC grid. Int J Electr Power Energy Syst 2023;145:108645.
[3] Yin C, Xie X, Liu H, Wang X, Wang Z, Chi Y. Analysis and control of the oscillation phenomenon in VSC-HVDC transmission system. Power Syst Technol 2018;43(3):1117–23.
[4] Yin C, Xie X, Xu S, Zou C. Review of oscillations in VSC-HVDC systems caused by control interactions. J Eng 2019;2019(16). 1204-07.
[5] Cheng Y, Fan L, Rose J, Huang F, Schmall J, Wang X, et al. Real-world subsynchronous oscillation events in power grids with high penetrations of inverter-based resources. IEEE Trans Power Syst 2023;38(1):316–30.
[6] Lyu J, Cai X, Amin M, Molinas M. Sub-synchronous oscillation mechanism and its suppression in MMC-based HVDC connected wind farms. IET Gener Trans Distr 2017;32(2). 458-70.
[7] Liu H, Sun J. Voltage stability and control of offshore wind farms with AC collection and HVDC transmission. IEEE J Emerg Sel Top Power Electron 2014;2(4). 1181-89.
[8] Wang Y, Zhao C, Guo C, Rehman AU. Dynamics and small signal stability analysis of PMSG-based wind farm with an MMC-HVDC system. CSEE J Power Energy Syst 2020;6(1):226–35.
[9] Shao B, Zhao S, Yang Y, Gao B, Blaabjerg F. Sub-synchronous oscillation characteristics and analysis of direct-drive wind farms with VSC-HVDC systems. IEEE Trans Sustain Energy 2021;12(2):1127–40.
[10] Du W, Fu Q, Wang H. Subsynchronous oscillations caused by open-loop modal coupling between VSC-based HVDC line and power system. IEEE Trans Power Syst 2018;33(4):3664–77.
[11] Kunjumuhammed LP, Pal BC, Gupta R, Dyke KJ. Stability analysis of a PMSG-based large offshore wind farm connected to a VSC-HVDC. IEEE Trans Energy Convers 2017;32(3):1166–76.
[12] Shao B, Zhao S, Gao B, Yang Y, Blaabjerg F. Adequacy of the single-generator equivalent model for stability analysis in wind farms with VSC-HVDC systems. IEEE Trans Energy Convers 2021;36(2):907–18.
[13] Shao B, Zhao S, Gao B, Yang Y, Blaabjerg F. An equivalent model for sub-synchronous oscillation analysis in direct-drive wind farms with VSC-HVDC systems. Int J Electr Power Energy Syst 2021;125:106498.
[14] Wu M, Xie L, Cheng L, Sun R. A study on the impact of wind farm spatial distribution on power system sub-synchronous oscillations. IEEE Trans Power Syst 2016;31(3):2154–62.
[15] Qu C, Yi T, Li H, Chen B. Closely spaced modes identification through modified frequency domain decomposition. Measurement 2018;2018(128):388–92.
[16] Seyranian AP. Sensitivity analysis of multiple eigenvalues. Mech Stru Machines 1993;21(2):261–84.
[17] Xiao X, Hu J. Low order vibration control for structures with highly correlated close modes. Sci China Technol Sci 2011;54(7):1855–64.
[18] Dobson I, Zhang J, Greene S, Engdahl H, Sauer PW. Is strong modal resonance a precursor to power system oscillations. IEEE Trans Circuits Syst I-Fundam Theor Appl 2001;48(3). 340-49.
[19] Dobson I, Barocio E. Perturbations of weakly resonant power system electromechanical modes. IEEE Trans Power Syst 2005; 20(1): 330–337.
[20] Du W, Chen X, Wang H. A method of open-loop modal analysis to examine the SSOs in a multi-machine power system with multiple variable-speed wind generators. IEEE Trans Power Syst 2018;33(4):4297–307.
[21] Shao B, Meng X, Han P, Yang Y, Wu H, Chen Z, et al. Participation factors instability and analysis of direct-drive wind farms with VSC-HVDC systems. In Proc IEEE PESGM 2022:1–5.
[22] Shair J, Xie X, Yan G. Mitigating subsynchronous control interaction in wind power systems: existing techniques and open challenges. Renew Sust Energ Rev 2019;108:330–46.
[23] Jyothsna TR, Vaisakh K. Effects of strong resonance in multimachine power systems with SSSC supplementary modulation controller. Int Trans Electr Energy Syst 2013;23(1):24–7.
[24] Gharebaghi M, Ghazi R. Proposed mechanism for performance of power system stabilizers in the condition of strong resonance. Int J Electr Power Energy Syst 2013;44(1):256–66.
[25] Padiyar KR, Prakash VS. Tuning and performance evaluation of damping controller for a STATCOM. Int J Electr Power Energy Syst 2003;25(2):155–66.
[26] Li P, Wu X, Zhang Y, Jin X, Xu A. Interaction and coordination of modulation controllers of multi-infeed HVDC in CSG. Automation of Electr Power Syst 2007;31(21):90–3.
[27] Chen S. Matrix perturbation theory in structural dynamic design. Beijing: Science Press; 2007.
[28] Kundur P. Power System Stability and Control. New York: McGraw-Hill; 1994.
[29] Seyranian AP. Collision of eigenvalues in linear oscillatory systems. J Appl Math Mech 1994;58(5):805–13.
[30] Shao B, Zhao S, Yang Y, Gao B, Wang L, Blaabjerg F. Nonlinear subsynchronous oscillation damping controller for direct-drive wind farms with VSC-HVDC systems. IEEE J Emerg Sel Top Power Electron 2022;10(3):2842–58.
[31] Shair J, Xie X, Yang J, Li J, Li H. Adaptive damping control of subsynchronous oscillation in DFIG-based wind farms connected to series compensated network. IEEE Trans Power Deliv 2022;37(2):1036–49.
[32] Zheng B, Takamatsu J, Ikeuchi K. An adaptive and stable method for fitting implicit polynomial curves and surfaces. IEEE Trans Pattern Anal Mach Intell 2010;32(3).561-68.
[33] Du W, Zhen Z, Wang H. The subsynchronous oscillations caused by an LCC HVDC line in a power system under the condition of near strong modal resonance. IEEE Trans Power Del 2018;33(2):840–50.